Photoacoustic imaging platforms for multimodal imaging

ULTRA SONO GRAPHY

Jeesu Kim[1], Donghyun Lee[2], Unsang Jung[3], Chulhong Kim[1,2]

Departments of [1]Electrical Engineering and [2]Creative IT Engineering, [3]Future IT Innovation Laboratory, Pohang University of Science and Technology, Pohang, Korea

REVIEW ARTICLE

http://dx.doi.org/10.14366/usg.14062
pISSN: 2288-5919 • eISSN: 2288-5943
Ultrasonography 2015;34:88-97

Photoacoustic (PA) imaging is a hybrid biomedical imaging method that exploits both acoustical and optical properties and can provide both functional and structural information. Therefore, PA imaging can complement other imaging methods, such as ultrasound imaging, fluorescence imaging, optical coherence tomography, and multi-photon microscopy. This article reviews techniques that integrate PA with the above imaging methods and describes their applications.

Keywords: Photoacoustic imaging; Ultrasonography; Optical imaging; Tomography, optical coherence; Multi-photon microscopy

Received: December 17, 2014
Revised: February 9, 2015
Accepted: February 16, 2015

Correspondence to:
Chulhong Kim, PhD, Departments of Electrical Engineering and Creative IT Engineering, Pohang University of Science and Technology, 77 Cheongam-ro, Nam-gu, Pohang 790-784, Korea

Tel. +82-54-279-8892
Fax. +82-54-279-8899
E-mail: chulhong@postech.edu

How to cite this article:
Kim J, Lee D, Jung U, Kim C. Photoacoustic imaging platforms for multimodal imaging. Ultrasonography. 2015 Apr;34(2):88-97.

Introduction

Photoacoustic (PA) imaging is a hybrid biomedical imaging method that exploits both acoustical and optical properties. PA imaging has been evaluated as a preclinical and clinical imaging method in the biomedical field [1–6]. PA imaging is based on the PA effect [7]. When a pulsed laser with a pulse width of a few nanoseconds illuminates a target object, a PA wave can be induced as a consequence of the object's thermoelastic expansion and subsequent relaxation (Fig. 1) [2]. An ultrasound (US) transducer detects the PA wave, and an image is reconstructed through an imaging process. The initial pressure *P* (Pa) of a generated PA wave can be expressed as

$$P \propto \Gamma(T)\,\sigma\mu_a F\,, \tag{1}$$

where Γ is the temperature-dependent Grueneisen parameter, σ $(0 \le \sigma \le 1)$ (dimensionless) is the heat conversion efficiency, μ_a (1/cm) is the optical absorption coefficient, and *F* (W/m^2) is the optical fluence. All of these parameters are directly proportional to PA amplitude, and therefore increasing one or more of the parameters can increase PA amplitude.

The PA wave equation can be expressed as

$$\frac{1}{v_s}\frac{\partial^2 p(\vec{r}_0,t)}{\partial t^2} - \nabla^2 p(\vec{r}_0,t) = \frac{\beta}{C_p}\frac{\partial H(\vec{r},t)}{\partial t}\,, \tag{2}$$

where v_s (m/sec) is the sound velocity in the medium, $p(\vec{r},t)$ (Pa) is the PA wave pressure at location $\vec{r}$ and time t, β (dV/K) is the volumetric thermal expansion coefficient, C_p (J/kg/K) is the heat conversion capacity, and *H* is the heating function of thermal energy conversion [8]. The generated PA wave, which is represented by the left-hand side of Eq (2), depends on variation in the heating source,

which is represented by the right-hand side of Eq (2). The pressure of the PA wave increases with the rate of variation of the heat source. In order to generate PA waves effectively, the width of the laser pulse should be sufficiently smaller than the thermal and stress relaxation times. For example, a spherical object with a diameter of 15 μm has a thermal time of 1.7 milliseconds and a stress relaxation time of 10 nanoseconds in soft tissue. Two main PA imaging techniques are used: PA tomography (PAT) and PA microscopy (PAM) [2,6,9]. PAT uses array-type transducers (e.g., linear, arc, or circular array) and a mathematical image reconstruction algorithm to form a PA image [10–15]. Although PAT systems using array-type transducers can provide real-time imaging capability, the reconstructed PAT images include artifacts caused by the imperfect reconstruction algorithm. Therefore, the main challenge in PAT is to improve image quality by reducing these artifacts [16–19]. PAM uses a single-element focused US transducer and acquires one-dimensional depth information at one location. To acquire three-dimensional volumetric information, mechanical or optical raster scanning is required [20,21]. PAM can provide a PA image with high spatial resolution by sacrificing imaging speed.

PA imaging integrates the advantages of US and optical imaging. The penetration depth of PA imaging is up to 8 cm, whereas that of pure optical imaging techniques is up to 1 mm. PA imaging does not have speckle artifacts, whereas pure US does. PA imaging can also provide physiological information such as hemoglobin concentration, hemoglobin oxygen saturation, and angiogenesis. Therefore, PA imaging can provide additional complementary information when combined with other imaging methods such as US [22], fluorescence (FL) [23], optical coherence tomography (OCT) [24], and multi-photon microscopy (MPM) [25]. This review will describe techniques that integrate PA with the above imaging methods and discuss their applications.

US and PA imaging

US imaging is widely used in the biomedical field because it uses nonionizing acoustic radiation and can therefore provide real-time *in vivo* images without any risk of damage. However, its images suffer from intrinsic speckle artifacts that degrade the image quality. PA images do not contain speckle artifacts, so high-contrast images can be acquired. PA imaging can provide physiological information, such as hemoglobin concentration, hemoglobin oxygen saturation, and angiogenesis, as well as structural information. Therefore, PA imaging can provide information complementary to US when the two techniques are used in combination.

Due to its intrinsic properties, PA imaging can be easily integrated with clinical US machines [10–13,26–29]. In order to acquire a PA image, the radio frequency signal sequences of a clinical US machine must be modified. In US imaging, a transducer transmits US waves and receives the reflected US echoes. However, in PA imaging, the laser irradiation induces acoustic waves in the medium, so the US transducer only needs to receive the generated PA waves, instead of transmitting US waves. Therefore, the transmitting function of a clinical US system must be blocked in order to acquire a PA image. Furthermore, the beamforming algorithm must be modified to enable one-way detection. In order to modify the beamforming algorithm, the raw data of the received PA signal must be accessible. Thus, a US system can be modified to provide PA/US imaging ability by simply adding a pulsed laser source (Fig. 2A) [10].

The wavelength of a neodymium-doped yttrium aluminum garnet pump laser is tuned by a dye laser, so that the user can select an appropriate wavelength of light for obtaining PA signals of the target object. The output of the laser is coupled with a bifurcated fiber bundle, which is adapted with a US transducer probe. Pulsed laser beams are delivered by the fiber bundle to excite the target object. The excited object generates PA waves, which propagate omnidirectionally, such that the US transducer can receive them. The received PA signals are acquired by a data acquisition system and processed to construct a PA/US image. The integrated PA/US imaging system can provide both functional and structural information about biological tissues.

The sentinel lymph node of a rat was imaged *in vivo* using an integrated dual-modal PA/US imaging system (Fig. 2B) [11]. Methylene blue was injected into the forepaw to increase optical absorption contrast in the sentinel lymph node, and PA and US images were then acquired and overlaid. In order to increase the imaging depth, 2 cm of chicken tissue was laid on the rat. Pseudocolor was used to represent the PA image that shows the optical absorption contrast, and grayscale was used to represent the US image that shows the structure of surrounding tissues. The sentinel lymph node and major blood vessels were clearly distinguishable in the PA image, and the internal structures of the rat were visible in the US image. The combined PA/US image provided both functional information, such as methylene blue accumulation in the sentinel lymph node, and structural information, such as the shape of the surrounding tissue.

By exploiting well-developed US technology, PA imaging capability can be easily added to a clinical US imaging scanner. Typically, US imaging provides morphological information whereas PA imaging supplies physiological information.

FL and PA imaging

FL imaging is a nonionizing and inexpensive technique with

applications in molecular imaging [23,30–32]. However, due to optical diffusion in biological tissues, the spatial resolution of FL imaging is poor when light penetrates beyond 1 mm. In contrast, PA imaging retains spatial resolution to a penetration depth >5 cm.

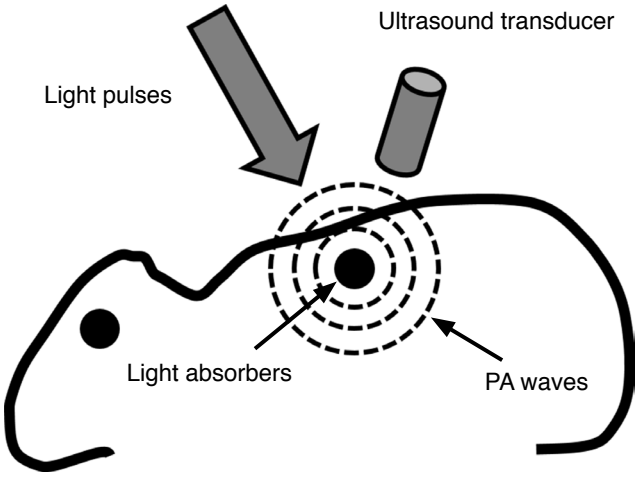

Fig. 1. **Schematic of photoacoustic imaging.** When a target absorbs pulsed light, photoacoustic (PA) waves are generated via thermoelastic expansion. The PA waves propagate and are detected by an ultrasound transducer. Reprinted from Kim et al. Chem Rev 2010;110:2756-2782 [2], with permission of American Chemical Society.

In general, the combination of FL and PA imaging uses exogenous contrast agents to visualize complementary optical absorption and FL properties of target objects. When irradiated by a laser source, an object gains energy, and then releases it either as light of another wavelength (i.e., FL) or as heat (i.e., a PA wave). The energy of FL depends on the FL quantum yield Y; the PA wave is generated by the remaining energy (i.e., 1–Y) [2]. Therefore, both PA and FL images of a target object can be acquired by injecting a single contrast agent that has an appropriate *Y*, so that the signal can be detected by both the FL and the PA imaging systems.

Indocyanine green has been used in combined PA and FL imaging [33,34]. *In vivo* PA and FL images of the bladder in rats were acquired after injecting indocyanine green [33]. The images were taken by separate PA and FL imaging systems (Fig. 3A, B). In the PA imaging system, pulsed laser beams with a pulse duration of 5 nanoseconds were generated by a 10-Hz Q-switched neodymium-doped yttrium aluminum garnet pump laser. The generated laser beams were tuned using an optical parametric oscillator system. The wavelength of the output laser can be tuned from 680 to 2,500 nm. The wavelength-tuned laser was delivered to a conical lens to make a donut-shaped beam pattern. A single-element focused US transducer was then placed in the center of the ring-shape beam. The diverged beam was refocused on the target object with an optical condenser. A bottom-open water tank and US gel were used to match acoustic impedance between the rat and the US transducer. The bottom of the

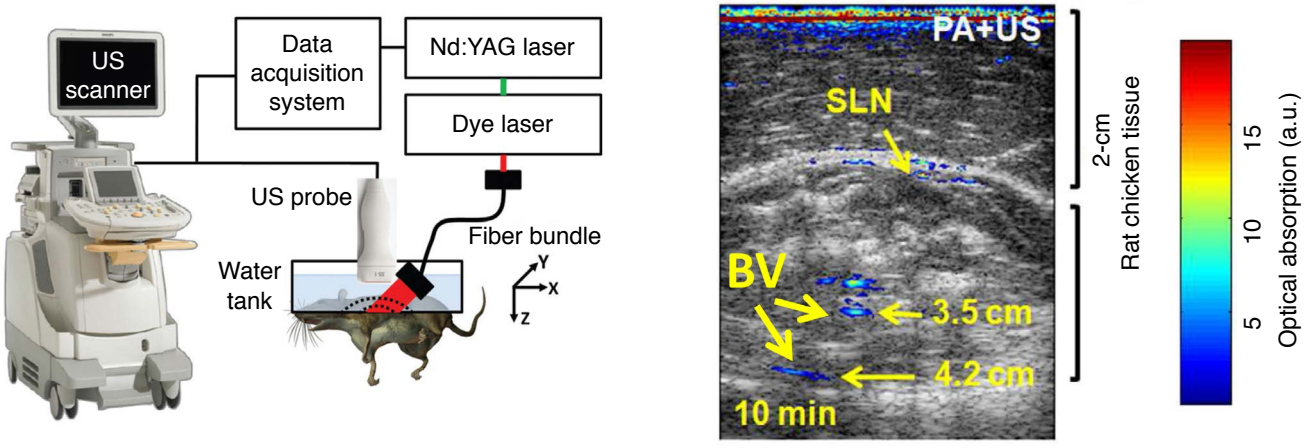

A B

Fig. 2. **Experimental setup of PA/US imaging system and example image.**
A. Schematic of integrated PA/US imaging system. The wavelength of the pumped laser is tuned by a dye laser and coupled with a fiber bundle. The fiber bundle is integrated with a US probe and excites target tissues. The generated PA waves are detected by US probe and saved by data acquisition system. B. The PA/US image of the SLN of the rat *in vivo*. Grayscale represents the sonogram and pseudo-color represents the PA image. PA signals from the SLN and BVs are indicated in (B). Nd:YAG, neodymium-doped yttrium aluminum garnet; PA, photoacoustic; US, ultrasound; SLN, sentinel lymph node; BV, blood vessel. Reprinted from Erpelding et al. Radiology 2010;256:102-110 [10], with permission of Radiological Society of North America; reprinted from Kim et al. Biomed Opt Express 2010;1:278-284 [11], with permission of The Optical Society.

water tank was sealed using a transparent membrane. The PA waves were detected by a US transducer, amplified, and saved by a data acquisition system. Mechanical raster scanning was used to acquire volumetric data. The PA image was constructed by post-processing the saved data. In the FL imaging system, a continuous-wave laser source was used. The output laser was filtered by an excitation filter, and then beamed directly at the target. The emitted FL signals were filtered by an emission filter and focused on a charge-coupled device camera, which detected the FL signals and constructed the FL image. Using this combination of PA and FL, *in vivo* bladder FL and PA images of the rat were acquired (Fig. 3C, D). Indocyanine green was injected through a 22-gauge lubricant-coated catheter. In general, the bladder itself does not have optical absorption, and is therefore invisible in a PA image. After injecting indocyanine green, the resulting PA image clearly showed the shape of bladder, as well as surrounding blood vessels (Fig. 3C). The FL image did not provide

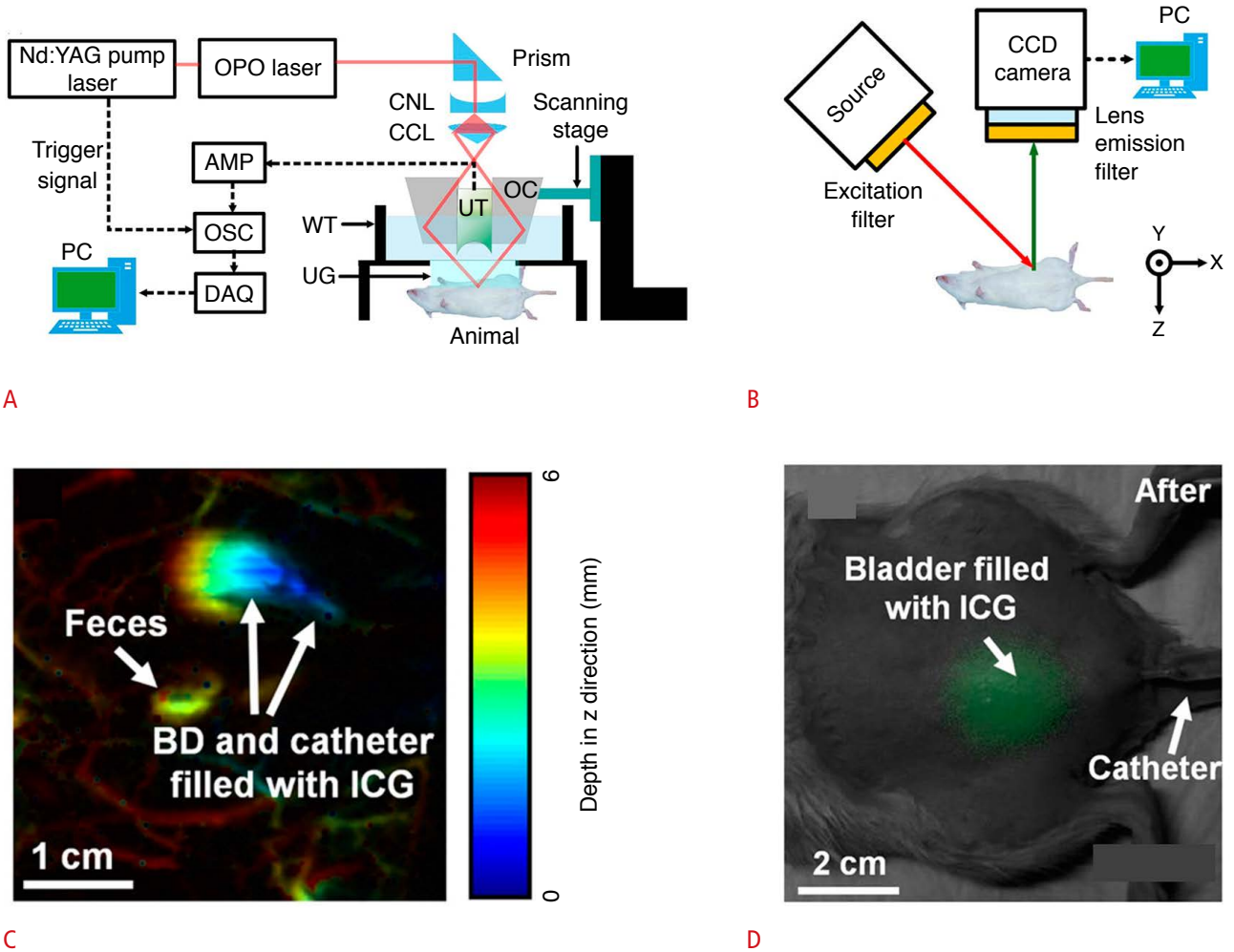

Fig. 3. Experimental setup of PA and FL imaging systems, and example image of each modality.
A. The wavelength of pumped laser is tuned by OPO laser and guided to CNL. CNL and CCL produce a ring-shaped beam and the OC merges the diverged beam to the target object. The UT detects the generated PA waves and the DAQ saves the detected signal. B. A filtered source laser excites the target tissue and the CCD camera detects the emitted FL signal. The FL signal is filtered by an emission filter. C. *In vivo* noninvasive PA images of an ICG injected bladder in a rat. Pseudo-color represents depth information (red=deep to blue=shallow). The PA signal from ICG in the bladder and catheter is clearly visible in (C). D. *In vivo* noninvasive PA images of ICG injected in the bladder of a rat. The grayscale picture is acquired under room light, and the green color represents the FL signal of the ICG. The background picture and FL image are acquired separately and overlaid in post-processing. Nd:YAG, neodymium-doped yttrium aluminum garnet; OPO, optical parametric oscillator; CNL, conical lens; CCL, concave lens; AMP, amplifier; OSC, oscilloscope; DAQ, data acquisition system; OC, optical condenser; UT, ultrasound transducer; WT, water tank; UG, ultrasound gel; PC, personal computer; BD, bladder; ICG, indocyanine green; PA, photoacoustic; FL, fluorescence. Reprinted from Park et al. Sensors (Basel) 2014;14:19660-19668 [33], according to the Creative Commons License MDPI.

structural information about the bladder but could verify that it took up indocyanine green (Fig. 3D).

Due to its low cost and use of nonionizing radiation, FL imaging has been evaluated for use in molecular imaging. However, due to strong light scattering, FL suffers from either poor spatial resolution or shallow penetration. Combined PA and FL imaging may become a vital technique in molecular imaging because it is safe, sensitive, inexpensive, and has high resolution.

PAM and OCT

PAM and OCT are both noninvasive microscopic optical imaging methods that exploit optical absorbance and optical scattering, respectively [35,36]. OCT uses a Michelson interferometer to perform low-coherence interferometry and can provide microstructural information with a resolution of 1–10 μm with an imaging depth of a few millimeters. OCT can also measure blood flow by exploiting the Doppler effect and optical polarization. Complementary information obtained using optical absorption and optical scattering can be provided by combining PAM and OCT imaging. In the integrated image, PAM provides functional information such as hemoglobin oxygen saturation, and OCT provides structural information about surrounding microstructures [35,37–39]. The most practical applications of the integrated PAM/OCT imaging system are in otolaryngology and ophthalmology. Conventional OCT has been predominantly used in ophthalmology because the optical transparency of the eye's cornea and lens greatly enhances the OCT imaging depth. In ophthalmology, OCT exploits optical scattering to provide structural information about the cornea, iris, and retina [40]. Further, OCT can even detect the multilayer structure in the retina, which is useful for diagnosing diabetic retinopathy. An integrated PAM/OCT imaging system can also provide optical absorption contrast information, such as retinal blood vessel distribution and hemoglobin oxygenation; this information can be useful in the diagnosis of retinal telangiectasia and Coats disease [41,42].

The integrated PAM/OCT imaging system is composed of three main parts: (1) the PAM system, (2) the OCT system, and (3) a dichroic mirror and two-dimensional galvanometer for beam

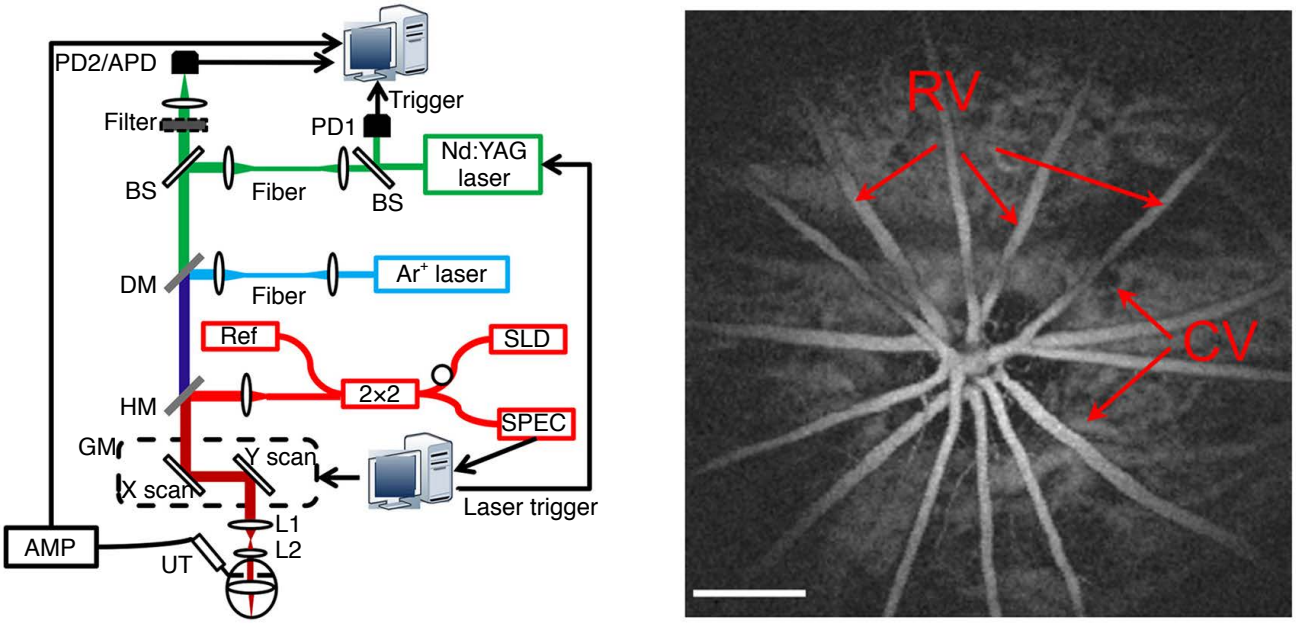

Fig. 4. Experimental setup of PAM/OCT imaging system and example image.
A. A tunable dye laser excites the target, and an unfocused needle transducer detects PA waves. A conventional spectral domain OCT system with broadband laser source, spectrometer and a line CCD camera are used to detect the interference signal in the spectral domain. The dichroic mirror combines the pulsed laser beam in the PAM system with the broadband laser beam in the OCT system. The two-dimensional galvanometer is used for raster scanning. B. Maximum amplitude projection PAM image of retinal vasculatures. Scale bar=500 μm. PD, photodiode; APD, avalanche photodetector; BS, beam splitter; Nd:YAG, neodymium-doped yttrium aluminum garnet; DM, dichroic mirror; HM, hot mirror; SLD, super luminescent diode; SPEC, spectrometer; GM, two-dimensional galvanometer; AMP, amplifier; UT, ultrasound transducer; RV, retina vessels; CV, choroidal vessels; PAM, photoacoustic microscopy; OCT, optical coherence tomography; PA, photoacoustic. Reprinted from Song et al. J Biomed Opt 2012;17:061206 [43], with permission of SPIE.

combining and scanning (Fig. 4A) [43,44]. In the PAM system, a tunable dye laser is used to excite the target optically, an unfocused needle transducer is used to detect PA waves, and a data acquisition board is used to digitize the data. The interference signal in the spectral domain is detected by a conventional spectral domain OCT system with a broadband laser source, spectrometer, and a line charge-coupled device camera. The dichroic mirror is used to combine the pulsed laser beam in the PAM system and the broadband laser beam in the OCT system. The two-dimensional galvanometer is used for raster scanning; it is synchronized with the data acquisition board and the OCT computer by reference to the external trigger signal from the PAM pulsed laser.

B-scan images of the retinal vasculature and choroid vessels in a rat were obtained using an integrated PAM/OCT imaging system. The maximum amplitude projection PAM image of the retinal vessels was also acquired (Fig. 4B). The integrated PAM/OCT imaging system provides both structural and functional information. Using PAM, the retinal oxygen saturation value can be measured using multi-wavelength scanning. Furthermore, the OCT system can measure the blood flow velocity by exploiting the Doppler effect.

The integrated PAM/OCT system can be simplified by using one light source for both PAM and OCT. Optical coherence PAM uses a broadband neodymium-doped yttrium aluminum garnet pulsed laser source [45]: a 532-nm wavelength pulsed laser beam is used for PAM, and a laser beam with a 580-nm center wavelength and 20-nm bandwidth is used for OCT. Another method for simple implementation uses a noncontact US signal detection approach [46]. By replacing the piezoelectric US transducer with an interferometer, the PA signal can be detected without touching the transducer to the sample. The advantage of this approach is that the interferometer can be also used for OCT. Therefore, noncontact PAM and OCT imaging systems can be combined easily.

OCT is an imaging method that is based on optical scattering and is widely utilized to acquire micron-scale structural information about biological tissues. PA imaging can provide additional physiological information about target objects. Therefore, a comprehensive range of information can be obtained by combining OCT and PAM, including tissue anatomy, hemoglobin concentration, blood flow, and saturated oxygen values.

PAM and MPM

MPM uses a low-energy wavelength laser for FL imaging of living cells and microscopic objects [47,48]. MPM exploits the fact that the FL effect is confined to a volume of less than one picoliter; therefore, the system can acquire a high-resolution FL image without using a pinhole. In this case, a nonlinear effect can occur due to the very rare instances in which a molecule absorbs more than one photon simultaneously. MPM has the advantage that it causes less photobleaching than conventional FL microscopy. MPM works by stimulating a target that has been labeled using a fluorescent dye, fluorescent proteins, nanoparticles, or specific natural fluorescent materials. Therefore, the targeted imaging of specific molecules is possible. Functional activity information about living tissue can also be obtained.

MPM is used in the biomedical field for molecular imaging, neuroscience, and cancer detection. MPM provides molecular information, such as the levels of reactive oxygen species, glutamate, NADH, FAD, and oxygen. MPM can also visualize the structural and physiological properties of cells, complex neural circuits, nerve activities, and blood flow [49], and can provide fluorescent images in a deeper area than can existing FL microscopy. MPM achieves a wide wavelength-tuning range (690–1,050 nm) by using a titanium-sapphire laser. The PAM laser has also a wide wavelength-tuning range (350–750 nm) that overlaps with the range of the MPM system. These advantages enable the acquisition of various functional information for targeted imaging.

PAM and MPM are high-resolution imaging technologies that can provide structural and physiological information of cells at a depth level in the millimeter range [50–52]. The two techniques were developed separately, but have recently been combined to improve diagnosis and analysis at high contrast. Combined technologies, such as OCT/MPM, OCT/PAT, US/PA, and confocal/MPM, will combine the strengths of these technologies and compensate for their individual weaknesses [53,54].

Recently, a new integrated system has been developed, combining PAM, confocal microscopy, and MPM [25]. This means that MPM can be extended to new biological investigations by measuring nonfluorescent substances such as hemoglobin and melanin. In the combined system (Fig. 5A), two polarization beam splitters and a half-wave plate combine the optical source of each technology into an optical common path in a commercial microscope. The PA signals generated by the sample are detected by an acoustic transducer in the microscope body. Dichroic mirrors then split the backward-propagating fluorescent light into two beams. One is sent to the confocal detector and one is sent to the MPM signal detector. Images of moss leaves were acquired: the MPM image visualized leaf cell boundaries and chloroplasts inside the leaf cells (Fig. 5B), a confocal image was obtained based on FL signals from the chloroplasts (Fig. 5C), and the optical resolution PAM maximum amplitude projection images visualized the moss leaves at optical wavelengths of 570 nm (Fig. 5D) and 578 nm (Fig. 5E). The maximum amplitude images of the MPM, confocal microscopy, and 570-nm optical-resolution PAM systems were merged into one overlay as green, red, and

blue, respectively (Fig. 5F), and a differential absorption contrast image was generated in order to visualize the change in optical absorption across multiple wavelengths (Fig. 5G). The differential absorption contrast images can provide functional information about nonfluorescent chromophores.

Optical absorption and FL targets can be imaged simultaneously using combined PA and FL imaging systems. This approach can also be applied to microscopic imaging technologies. The beauty of dual-mode PAM and MPM is that the combined imaging system can show both fluorescent and non-fluorescent chromophores at a micron scale.

Summary

The multimodal capability of PA imaging techniques was reviewed. PA imaging is a noninvasive and nonionizing imaging method that is based on both optical absorption and the generation of acoustic waves by thermoelastic expansion. PA imaging is safe, fast, and inexpensive. A PA imaging system can be easily integrated with various imaging modalities such as US, FL, OCT, and MPM. The strengths of PA imaging complement the weaknesses of each of the above imaging methods. Furthermore, integrated systems can provide structural information (i.e., surrounding blood vessels, organs, and microstructures), physiological information (i.e., hemoglobin concentration, hemoglobin oxygen saturation, and angiogenesis), and molecular information (i.e., exogenous contrast agent uptake). PA imaging could also potentially be integrated with other biomedical imaging methods, including magnetic resonance imaging, computed tomography, positron emission tomography, and single photon emission computed tomography.

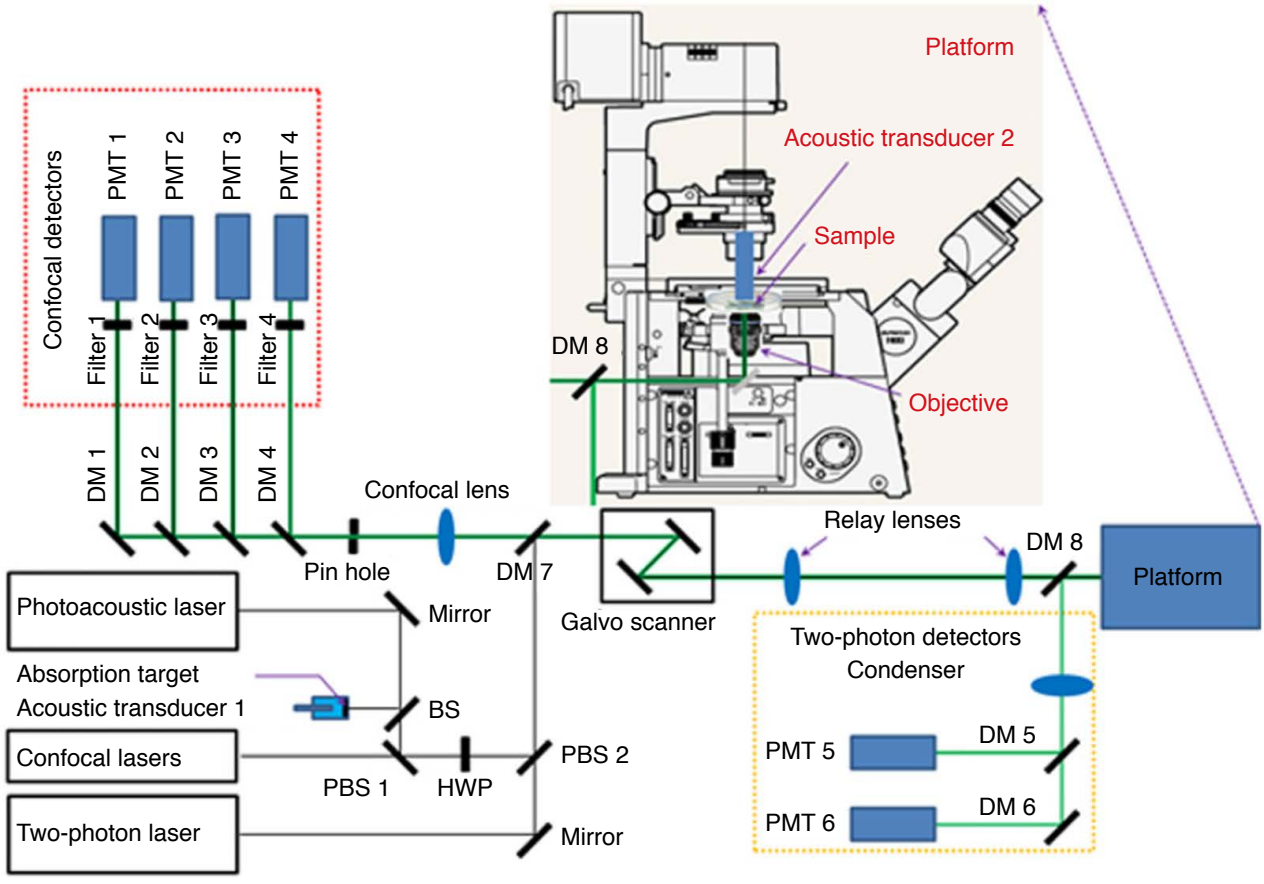

A

Fig. 5. Experimental setup of the combined confocal, two-photon, and optical-resolution microscope, and example images.
A. Two polarization beam splitters and a half-wave plate combine the optical sources into a common optical path in a commercial microscope. The generated PA signals are detected by an acoustic transducer in the microscope. Then dichroic mirrors split the backward-propagating fluorescent light into two beams; one is sent to the confocal detector, and the other is sent to the MPM signal detector.

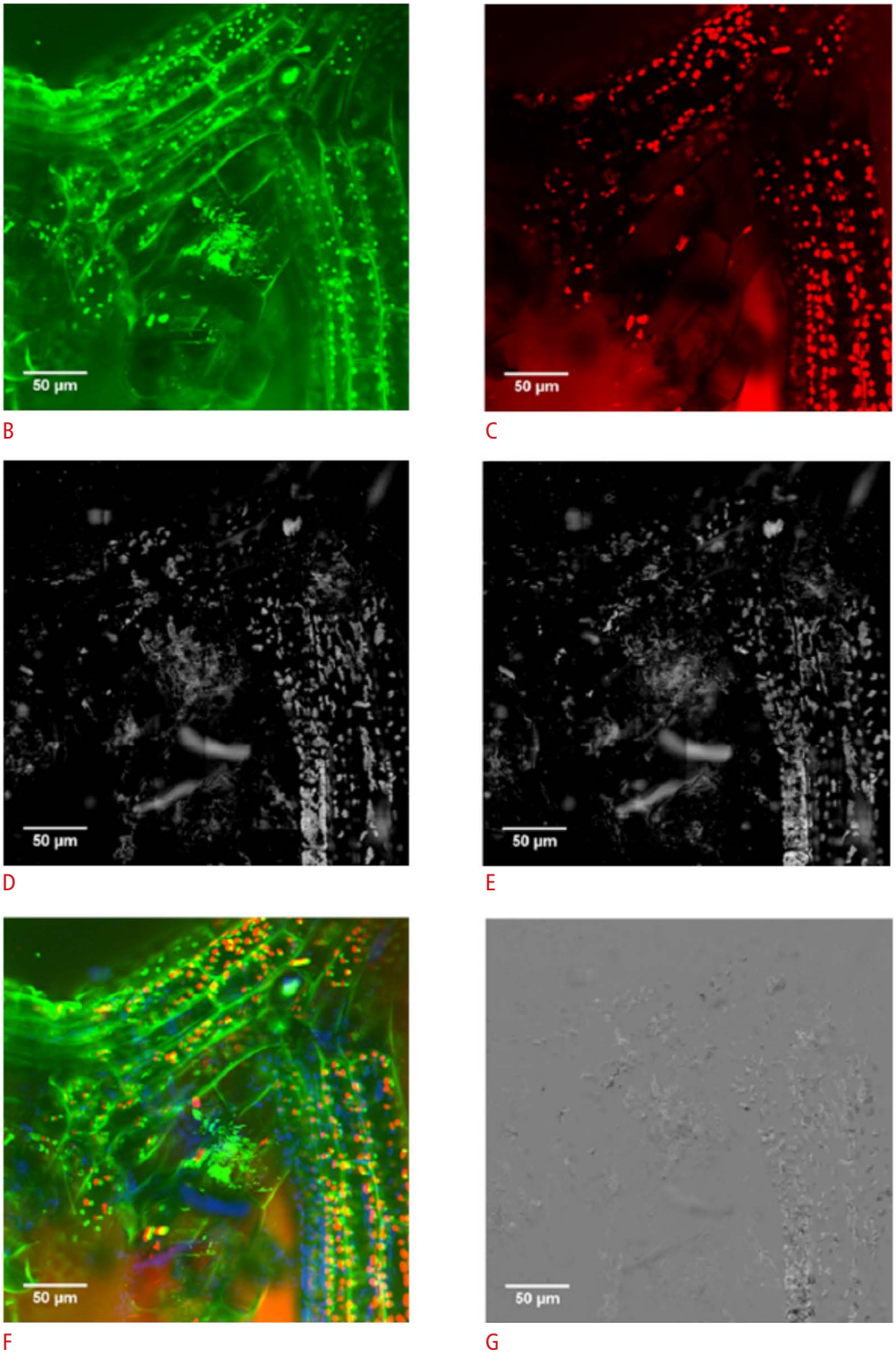

Fig. 5. B. MPM image of leaf cell boundaries and chloroplasts. C. Confocal image of FL signals from chloroplasts. D. OR-PAM MAP image of moss leaves at 570 nm. E. OR-PAM MAP image of the moss leaves at 578 nm. F. Merged image rendered from MPM, confocal, and 570 nm OR-PAM image as green, red, and blue color respectively. G. Differential absorption contrast image of OR-PAM MAP image. PMT, photomultiplier tube; DM, dichroic mirror; BS, beam splitter; PBS, polarization beam splitter; HWP, half-wave plate; PA, photoacoustic; MPM, multi-photon microscopy; FL, fluorescence; OR-PAM, optical-resolution photoacoustic microscopy; MAP, maximum amplitude projection. Reprinted from Rao et al. J Biomed Opt 2014;19:36002 [25], with permission of SPIE.

ORCID: Jeesu Kim: http://orcid.org/0000-0002-2542-0234; Donghyun Lee: http://orcid.org/0000-0002-8015-8574; Unsang Jung: http://orcid.org/0000-0002-0814-5357; Chulhong Kim: http://orcid.org/0000-0001-7249-1257

Conflict of Interest
No potential conflict of interest relevant to this article was reported.

Acknowledgments
This work was supported by the research funds from the following grants: NRF-2013K1A3A1A20046921 (China-ROK Joint Research Project), NRF-2011-0030075 (Engineering Research Center), NRF-2014M3C1A3017229 (NRF Pioneer Research Center Program), and NIPA-2014-H0201-14-1001 (IT Consilience Creative Program of the Ministry of Science, ICT and Future Planning [MSIP], Republic of Korea).

References

1. Beard P. Biomedical photoacoustic imaging. Interface Focus 2011;1:602-631.
2. Kim C, Favazza C, Wang LV. In vivo photoacoustic tomography of chemicals: high-resolution functional and molecular optical imaging at new depths. Chem Rev 2010;110:2756-2782.
3. Jeon M, Kim C. Multimodal photoacoustic tomography. IEEE Trans Multimed 2013;15:975-982.
4. Mallidi S, Luke GP, Emelianov S. Photoacoustic imaging in cancer detection, diagnosis, and treatment guidance. Trends Biotechnol 2011;29:213-221.
5. Wang LV, Hu S. Photoacoustic tomography: in vivo imaging from organelles to organs. Science 2012;335:1458-1462.
6. Wang LV. Tutorial on photoacoustic microscopy and computed tomography. IEEE J Sel Top Quantum Electron 2008;14:171-179.
7. Bell AG. The photophone. Science 1880;1:130-134.
8. Xu M, Wang LV. Universal back-projection algorithm for photoacoustic computed tomography. Phys Rev E Stat Nonlin Soft Matter Phys 2005;71:016706.
9. Wang LV. Multiscale photoacoustic microscopy and computed tomography. Nat Photonics 2009;3:503-509.
10. Erpelding TN, Kim C, Pramanik M, Jankovic L, Maslov K, Guo Z, et al. Sentinel lymph nodes in the rat: noninvasive photoacoustic and US imaging with a clinical US system. Radiology 2010;256:102-110.
11. Kim C, Erpelding TN, Jankovic L, Pashley MD, Wang LV. Deeply penetrating in vivo photoacoustic imaging using a clinical ultrasound array system. Biomed Opt Express 2010;1:278-284.
12. Kim C, Erpelding TN, Jankovic L, Wang LV. Performance benchmarks of an array-based hand-held photoacoustic probe adapted from a clinical ultrasound system for non-invasive sentinel lymph node imaging. Philos Trans A Math Phys Eng Sci 2011;369:4644-4650.
13. Kim C, Erpelding TN, Maslov K, Jankovic L, Akers WJ, Song L, et al. Handheld array-based photoacoustic probe for guiding needle biopsy of sentinel lymph nodes. J Biomed Opt 2010;15:046010.
14. Gamelin J, Maurudis A, Aguirre A, Huang F, Guo P, Wang LV, et al. A real-time photoacoustic tomography system for small animals. Opt Express 2009;17:10489-10498.
15. Gamelin J, Aguirre A, Maurudis A, Huang F, Castillo D, Wang LV, et al. Curved array photoacoustic tomographic system for small animal imaging. J Biomed Opt 2008;13:024007.
16. Xu Y, Feng D, Wang LV. Exact frequency-domain reconstruction for thermoacoustic tomography: I. Planar geometry. IEEE Trans Med Imaging 2002;21:823-828.
17. Wang X, Xu Y, Xu M, Yokoo S, Fry ES, Wang LV. Photoacoustic tomography of biological tissues with high cross-section resolution: reconstruction and experiment. Med Phys 2002;29:2799-2805.
18. Xu Y, Wang LV, Ambartsoumian G, Kuchment P. Reconstructions in limited-view thermoacoustic tomography. Med Phys 2004;31:724-733.
19. Zhang C, Wang Y. A reconstruction algorithm for thermoacoustic tomography with compensation for acoustic speed heterogeneity. Phys Med Biol 2008;53:4971-4982.
20. Maslov K, Stoica G, Wang LV. In vivo dark-field reflection-mode photoacoustic microscopy. Opt Lett 2005;30:625-627.
21. Kim C, Jeon M, Wang LV. Nonionizing photoacoustic cystography in vivo. Opt Lett 2011;36:3599-3601.
22. Jeon M, Song W, Huynh E, Kim J, Kim J, Helfield BL, et al. Methylene blue microbubbles as a model dual-modality contrast agent for ultrasound and activatable photoacoustic imaging. J Biomed Opt 2014;19:16005.
23. Wang Y, Maslov K, Kim C, Hu S, Wang LV. Integrated photoacoustic and fluorescence confocal microscopy. IEEE Trans Biomed Eng 2010;57:2576-2578.
24. Cai X, Zhang Y, Li L, Choi SW, MacEwan MR, Yao J, et al. Investigation of neovascularization in three-dimensional porous scaffolds in vivo by a combination of multiscale photoacoustic microscopy and optical coherence tomography. Tissue Eng Part C Methods 2013;19:196-204.
25. Rao B, Soto F, Kerschensteiner D, Wang LV. Integrated photoacoustic, confocal, and two-photon microscope. J Biomed Opt 2014;19:36002.
26. Wang K, Xia J, Li C, Wang LV, Anastasio MA. Fast spatiotemporal image reconstruction based on low-rank matrix estimation for dynamic photoacoustic computed tomography. J Biomed Opt 2014;19:056007.
27. Harrison T, Ranasinghesagara JC, Lu H, Mathewson K, Walsh A, Zemp RJ. Combined photoacoustic and ultrasound biomicroscopy. Opt Express 2009;17:22041-22046.
28. Karpiouk AB, Aglyamov SR, Mallidi S, Shah J, Scott WG, Rubin JM, et al. Combined ultrasound and photoacoustic imaging to detect

and stage deep vein thrombosis: phantom and ex vivo studies. J Biomed Opt 2008;13:054061.
29. Kolkman RG, Brands PJ, Steenbergen W, van Leeuwen TG. Real-time in vivo photoacoustic and ultrasound imaging. J Biomed Opt 2008;13:050510.
30. Lovell JF, Jin CS, Huynh E, Jin H, Kim C, Rubinstein JL, et al. Porphysome nanovesicles generated by porphyrin bilayers for use as multimodal biophotonic contrast agents. Nat Mater 2011;10:324-332.
31. Akers WJ, Kim C, Berezin M, Guo K, Fuhrhop R, Lanza GM, et al. Noninvasive photoacoustic and fluorescence sentinel lymph node identification using dye-loaded perfluorocarbon nanoparticles. ACS Nano 2011;5:173-182.
32. Akers WJ, Edwards WB, Kim C, Xu B, Erpelding TN, Wang LV, et al. Multimodal sentinel lymph node mapping with single-photon emission computed tomography (SPECT)/computed tomography (CT) and photoacoustic tomography. Transl Res 2012;159:175-181.
33. Park S, Kim J, Jeon M, Song J, Kim C. In vivo photoacoustic and fluorescence cystography using clinically relevant dual modal indocyanine green. Sensors (Basel) 2014;14:19660-19668.
34. Kim C, Song KH, Gao F, Wang LV. Sentinel lymph nodes and lymphatic vessels: noninvasive dual-modality in vivo mapping by using indocyanine green in rats: volumetric spectroscopic photoacoustic imaging and planar fluorescence imaging. Radiology 2010;255:442-450.
35. Jiao S, Xie Z, Zhang HF, Puliafito CA. Simultaneous multimodal imaging with integrated photoacoustic microscopy and optical coherence tomography. Opt Lett 2009;34:2961-2963.
36. Lee C, Han S, Kim S, Jeon M, Jeon MY, Kim C, et al. Combined photoacoustic and optical coherence tomography using a single near-infrared supercontinuum laser source. Appl Opt 2013;52:1824-1828.
37. Liu T, Wei Q, Wang J, Jiao S, Zhang HF. Combined photoacoustic microscopy and optical coherence tomography can measure metabolic rate of oxygen. Biomed Opt Express 2011;2:1359-1365.
38. Yang Y, Li X, Wang T, Kumavor PD, Aguirre A, Shung KK, et al. Integrated optical coherence tomography, ultrasound and photoacoustic imaging for ovarian tissue characterization. Biomed Opt Express 2011;2:2551-2561.
39. Zhang EZ, Povazay B, Laufer J, Alex A, Hofer B, Pedley B, et al. Multimodal photoacoustic and optical coherence tomography scanner using an all optical detection scheme for 3D morphological skin imaging. Biomed Opt Express 2011;2:2202-2215.
40. Mujat M, Ferguson RD, Patel AH, Iftimia N, Lue N, Hammer DX. High resolution multimodal clinical ophthalmic imaging system. Opt Express 2010;18:11607-11621.
41. Jiao S, Jiang M, Hu J, Fawzi A, Zhou Q, Shung KK, et al. Photoacoustic ophthalmoscopy for in vivo retinal imaging. Opt Express 2010;18:3967-3972.
42. Zhang HF, Puliafito CA, Jiao S. Photoacoustic ophthalmoscopy for in vivo retinal imaging: current status and prospects. Ophthalmic Surg Lasers Imaging 2011;42 Suppl:S106-S115.
43. Song W, Wei Q, Liu T, Kuai D, Burke JM, Jiao S, et al. Integrating photoacoustic ophthalmoscopy with scanning laser ophthalmoscopy, optical coherence tomography, and fluorescein angiography for a multimodal retinal imaging platform. J Biomed Opt 2012;17:061206.
44. Liu W, Zhang HF. Noninvasive in vivo imaging of oxygen metabolic rate in the retina. In: Engineering in Medicine and Biology Society (EMBC), 2014 36th Annual International Conference of the IEEE Engineering in Medicine and Biology Society 2014; Aug 26-30; Chicago, IL, USA. Piscataway, NJ: IEEE, 2014;3865-3868.
45. Zhang X, Zhang HF, Jiao S. Optical coherence photoacoustic microscopy: accomplishing optical coherence tomography and photoacoustic microscopy with a single light source. J Biomed Opt 2012;17:030502.
46. Hochreiner A, Bauer-Marschallinger J, Burgholzer P, Jakoby B, Berer T. Non-contact photoacoustic imaging using a fiber based interferometer with optical amplification. Biomed Opt Express 2013;4:2322-2331.
47. Denk W, Strickler JH, Webb WW. Two-photon laser scanning fluorescence microscopy. Science 1990;248:73-76.
48. Oheim M, Michael DJ, Geisbauer M, Madsen D, Chow RH. Principles of two-photon excitation fluorescence microscopy and other nonlinear imaging approaches. Adv Drug Deliv Rev 2006;58:788-808.
49. Chen Y, Guo H, Gong W, Qin L, Aleyasin H, Ratan RR, et al. Recent advances in two-photon imaging: technology developments and biomedical applications. Chin Opt Lett 2013;11:011703.
50. Shelton RL, Applegate BE. Ultrahigh resolution photoacoustic microscopy via transient absorption. Biomed Opt Express 2010;1:676-686.
51. Kobat D, Horton NG, Xu C. In vivo two-photon microscopy to 1.6-mm depth in mouse cortex. J Biomed Opt 2011;16:106014.
52. Helmchen F, Denk W. Deep tissue two-photon microscopy. Nat Methods 2005;2:932-940.
53. Tang S, Krasieva TB, Chen Z, Tromberg BJ. Combined multiphoton microscopy and optical coherence tomography using a 12-fs broadband source. J Biomed Opt 2006;11:020502.
54. Graf BW, Boppart SA. Multimodal skin imaging with integrated optical coherence and multiphoton microscopy. IEEE J Sel Top Quantum Electron 2012;18:1280-1286.